ISSN 1330-3651
UDC/UDK 62-837:531.35]:004.942

MODELLING AND SIMULATION OF DYNAMIC BEHAVIOUR OF ELECTRIC MOTOR DRIVEN MECHANISMS

Zoran Marinković, Dragan Marinković, Goran Petrović, Predrag Milić

Original scientific paper

The paper reviews simplified equivalent torsional models as an efficient approach to modelling and simulating dynamic behaviour of electric motor driven mechanisms. The focus is put on preliminary design phase. Motion of the masses is described by a system of second-order non-homogeneous differential equations. The solution yields the law of motion as well as the torque function in the elastic bonds between the masses. Special attention is dedicated to accurate modelling of electric motor characteristics and resistant forces acting on executive parts of drive mechanisms. Stochastic nature of resistant forces is also considered. The aim is to demonstrate that the combination of a simplified model with an accurate description of drive and load torques produces satisfactory results, which are, therefore, useful in furthering the design process. Two examples involving drive mechanisms of a crane and a bucket-wheel excavator illustrate the approach.

Keywords: *electric motor drive, equivalent torsional model, simulation, crane, bucket-wheel excavator*

Modeliranje i simulacija dinamičkog ponašanja mehanizama pogonjenih elektromotorom

Izvorni znanstveni članak

Članak preispituje pojednostavnjene ekvivalentne torzijske modele kao učinkoviti pristup modeliranju i simuliranju dinamičkog ponašanja mehanizama pogonjenih elektromotorom. Naglasak je stavljen na početnu fazu konstruiranja. Gibanje masa je opisano pomoću sustava nehomogenih diferencijalnih jednadžbi drugog reda. Rješenje donosi zakon gibanja kao i funkciju momenta u elastičnim vezama između masa. Posebna pozornost posvećena je preciznom modeliranju karakteristika elektromotora i sila otpora koje djeluju na izvršne dijelove pogonskih mehanizama. Također se razmatra stohastička priroda sila otpora. Cilj je pokazati da kombinacija pojednostavnjenog modela s točnim opisom pogona i opterećenja momentima proizvodi zadovoljavajuće rezultate, koji su, dakle, korisni u unapređivanju procesa konstruiranja. Dva primjera koji uključuju pogonske mehanizme dizalice i rotorskog bagera ilustriraju pristup.

Ključne riječi: *elektromotorni pogon, ekvivalentni torzijski model, simulacija, dizalica, rotorski bager*

1 Introduction

Electric motor drive is used by a number of machines, e.g.: machines of discontinuous transport (cranes, elevators), machines of continuous transport (transporters, conveyors), bucket-wheel excavators, tool machines, etc. It is an electro-mechanical system consisting of a group of components that converts electric into mechanical energy and delivers it to the executive parts of machines.

Gaining information about dynamic behaviour of drive mechanisms of these machines in different exploitation conditions is of crucial importance for their final design. This is achieved by modelling and simulating their work. Models with different level of complexity enable the engineer to address various physical phenomena involved in considered systems to different depth. Depending on the system that is to be designed, different design phases may require models of different levels of complexity.

In the preliminary design phase the aim is to define main parameters of the conceptual design. In this phase, the considered drive mechanisms are often handled by equivalent discrete torsional models. One of the major advantages of the approach resides in its simplicity, especially compared to models based on 3D geometry, such as FEM models. The FEM, as a most power numerical tool for structural analysis, is nowadays almost inevitably used in the detailed design phase. It can give a very detailed insight into the behaviour of mechanisms and accurate prediction of strain and stress states in single elements of drive mechanisms (e.g. [1, 2]), which accounts for its advantage. However, it requires relatively precise knowledge of geometry of analysed structures, expensive software, significant effort in modelling as well as computational effort since models typically have up to several 100 000 degrees of freedom. Discrete torsional models, on the other hand, are quite inexpensive in terms of modelling and computational effort and are applicable without quite precise knowledge of elements' geometry. They allow the engineer to assess the dynamic behaviour of drive mechanisms in the preliminary design phase. Based on the assessment, the engineer may proceed to the detailed design phase with the aim to revise design's basic parameters (for example, by means of FEM), or he may opt for another design concept.

Equivalent torsional models are not a novelty in the engineering community. They have been subject of interest of many authors within the last several decades (e.g. [3, 4, 5, 6, 7]) and their theoretical background is well established. The basic steps of deriving the model's parameters and resolving the laws of motion and loading functions are shortly addressed in the paper. The contribution the authors bring to the topic is related to accurate modelling of disturbances, which involves electric motor drive torque and resistant forces. Furthermore, they demonstrate that this leads to accurate predictions for speed of rotation and torque acting on mechanism's shafts.

Since the paper is application oriented, the approach is exemplified considering the already existing and fully functioning electric motor driven mechanisms of a crane and a bucket-wheel excavator. The comparison with experimental results is provided for the crane. Stochastic nature of resistant forces is considered for both mechanisms.

2
Equivalent torsional models of drive mechanisms

Model building, as one of the fundamental engineering activities, explores alternative solutions with the aim of achieving a satisfying compromise between the model complexity and the accuracy of predicted physical system's behaviour. It requires performing the following steps:

- deriving equivalent dynamic model,
- determination of model parameters and characteristics of external excitations,
- deriving adequate mathematical model,
- solving the mathematical model.

The steps are discussed in the sequel of the paper.

2.1
Equivalent dynamic model

A model has to describe the main aspects of physical behaviour of considered system according to objectives of modelling. The authors aim at a cost-effective approach that is to be applied in the preliminary design phase. Thus, complex mechanisms are modelled using equivalent torsional models. The principles of deriving equivalent dynamic model are illustrated considering electric motor driven mechanisms of a crane and a bucket-wheel excavator.

Fig. 1 depicts a drive mechanism of a laboratory apparatus, with the overall mass of 4,0 t and nominal speed of 1,08 m/s. The mechanism is used to simulate crane work. It consists of an AC squirrel cage electric motor, type KBF-90 LA 2, vertical three-stage reducer and a wheel placed on the output shaft of the reducer and running over the crane rail. The electric motor characteristics are: power P_M = 1,0 kW, revolutions per minute n_1 = 2510 min^{-1}, nominal torque T_n = 3,8 N·m and breaking torque T_B = 9,6 N·m. The reducer has a gear ratio of i_R = 35,5 and the wheel diameter is D = 250 mm. The velocity function $v(t)$ and torque function $T_{sh}(t)$ of the reference (output) shaft of the reducer are experimentally and analytically examined for a movement that consists of acceleration, stationary motion, braking and damping out vibrations after braking.

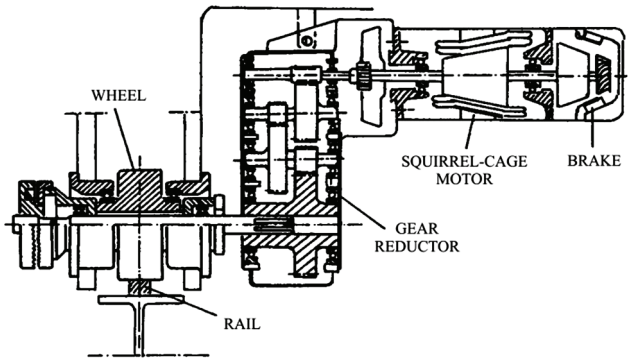

Figure 1 Drive mechanism of a laboratory apparatus for simulating cranes' movement

Similarly, Fig. 2 depicts the kinematic scheme of a drive mechanism of a bucket wheel excavator. It consists of an electric motor (1), elastic coupling with a brake (2), four-stage reducer (3) with a lamellar coupling (4) on the second shaft of the reducer and a bucket wheel (5) with 8 buckets.

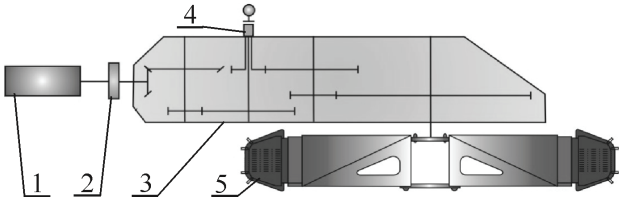

Figure 2 Drive mechanism of excavator's bucket wheel

In the first step, the considered real systems, i.e. drive mechanisms given in Figs. 1 and 2, are replaced by equivalent dynamic models. Generally speaking, those are combined models consisting of revolving and translating masses and elastic bonds between them. However, since the present analysis is focused on determination of shaft velocities and torques acting on shafts, the combined model is appropriately transformed into a torsional one consisting of concentrated revolving masses connected by elastic bonds. So, the concentrated masses represent revolving (rotor of the electric motor, gears of the reducer, etc.) and translating masses (wire-rope, grabbing device of the crane, etc.) of the machine and load (transported weight). The elastic bonds represent shafts and certain components of the executive part (e.g. the wire-rope).

In the first case, the equivalent torsional model consisting of 10 revolving masses and in the second case consisting of 11 revolving masses may be built. Of course, the number of elastic bonds would be less by 1. However, due to quite high stiffness of gear pairs, this coupling may be idealized as rigid, which reduces the size of both models to 7 revolving masses and 6 elastic bonds. Although numerical methods and powerful computer hardware make the dynamic behaviour of those models relatively easily tractable, the interest is most frequently focused on determination of torque load acting on one or a couple of shafts. This allows further model reduction.

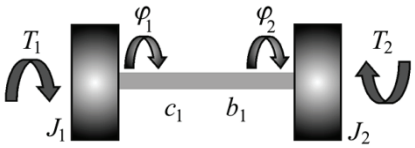

Figure 3 Equivalent discrete torsional model with only two revolving masses

Hence, in practice models with only 2 or 3 masses are quite often used. This is also a legacy from previous decades when PCs were not as powerful as today and the lack of user-friendly software was also a limiting factor. Equivalent torsional model with 2 revolving masses and 1 elastic bond, such as one in Fig. 3, is obtained through reduction of system characteristics onto a so-called reference shaft. Of course, the reduction may be performed for any shaft of the system and this is actually the shaft, for which the load torque function, $T_{sh}(t)$, is sought. Most often either the first – driving shaft or the last – output shaft is selected as a reference shaft.

The motion of considered mechanisms consists of three basic periods: acceleration, stationary motion and

deceleration (braking). However, a more realistic simulation of their motion requires decomposing the acceleration period into three phases and the braking period into two phases, so that overall six phases can be distinguished. According to the investigated phase even the model with only two masses can undergo certain modifications, actually further simplifications, as depicted in Fig. 4:

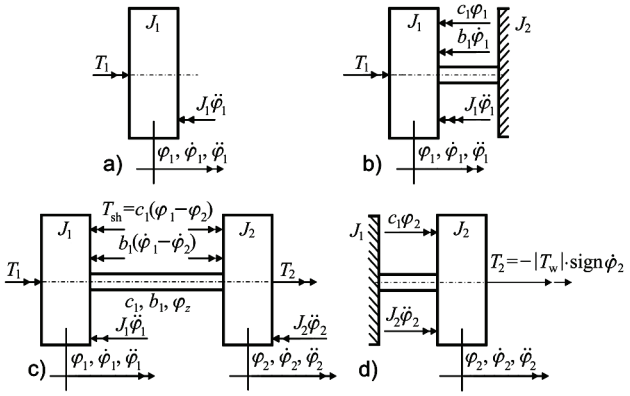

Figure 4 Modifications of equivalent torsional model with two revolving masses

- moving the first mass from the state of rest in order to close the gap in the mechanism (Fig. 4a),
- further acceleration of the first mass and deformation (torsion) of elastic connection until the second-driven mass starts to move (Fig. 4b),
- simultaneous asynchronous moving, i.e. acceleration of both masses (Fig. 4c),
- stationary-synchronous motion of both masses till the electric motor turns off and braking is initiated (Fig. 4c),
- braking - slowing down the first-driving mass until it rests (Fig. 4c),
- damping out vibrations of driven mass (Fig. 4d).

2.2 Model parameters and description of external disturbances

It is necessary to determine a set of parameters that define the equivalent torsional model. Once the reference shaft is chosen, it is necessary to perform the reduction of the following quantities and characteristics with respect to the reference shaft: inertia moments of rotors placed on other shafts, elastic and damping constants of other shafts, gaps and, finally, the torques acting on shafts other than the reference shaft. The procedure is based on equating the kinetic and potential energies of real and equivalent system [8]. In this manner all the masses up to the reference shaft form the driving mass described by the moment of inertia J_1 (kg·m^2), while the remaining masses form the driven mass J_2 (kg·m^2). The reference shaft, i.e. the elastic bond between the masses is described by the following characteristics: damping b_1 (N·m·s), stiffness c_1 (N·m) and gap φ_z (rad). They depend on the shape and dimensions of the elements as well as the material properties they are made of. Stiffness and damping alter in certain range during the work of the mechanisms, which is due to induced stresses, temperature field, variable velocity, etc., but in practice the models are linearized and, hence, the parameters are taken as constant values.

Both masses of the model are influenced by disturbing torques T_1 and T_2, the direction of which depends on the type of mechanism and movement phase. Thus, in the acceleration period, the driving mass is influenced by the positive torque of electric motor $T_1=T_M$ ($\dot{\varphi}$), and during the braking period the same mass is influenced by the negative torque created by the brake $T_1= -T_B(t)$. During the whole movement, the driven mass is influenced by load torque. Typically, the load torque acts in the direction opposite to the movement and is therefore often denoted as resistant torque. If that is the case, then the load torque is overcome by electric motor during the acceleration, while braking is facilitated by it. However, it should be kept in mind that, with some mechanisms, the load torque may also act in direction of movement. An example would be dropping of the load with a crane lift mechanism. Accurate description of the disturbing moments T_1 and T_2 is of crucial importance.

2.2.1 Modelling electric motor starting characteristic

The torque-speed curve of an electric motor depends on the type of motor, its starting and speed regulation. Nowadays, three-phase AC induction motors are widely used in industrial and commercial applications. They are classified either as squirrel cage or wound-rotor motors, the former rendering almost 90 % of the three-phase AC induction motors. This is the reason why squirrel cage electric motors are considered in this paper.

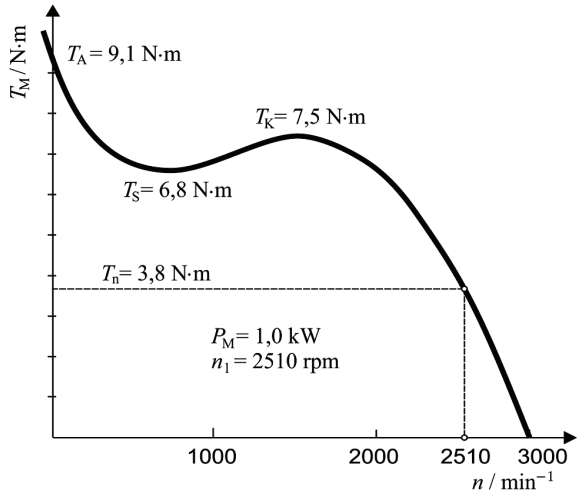

Figure 5 Torque-speed curve of squirrel cage motor KBF – 90 LA 2

Modelling the torque-speed curve of this type of motor will be considered on the example of motor KBF – 90 LA 2, Fig 5. This is a higher order curve given as a function of revolutions per minute $T_M(n)$ and which cannot be accurately enough described by a single analytical function. The motor at rest produces torque known as the locked rotor torque (T_A). As the motor accelerates, the torque first drops to a minimum torque, known as the pull-up torque (T_S), and then rises to a maximum torque, known as the pull-out torque (T_K). Those are actually the values specified by the producer.

In order to model the torque-speed curve, its two sections are treated separately: starting characteristic

between the locked rotor torque (T_A), and the pull-out torque (T_K); and the running characteristic starting at the point of the pull-out torque (T_K) and up to the synchronous speed. The first section can be described by a 4th order polynomial:

$$T_{M1}(n) = A_4 \cdot n^4 + A_3 \cdot n^3 + A_2 \cdot n^2 + A_1 \cdot n + A_0. \quad (1)$$

Since three points of the curve are known – T_A, T_S and T_K, as well as two points in which the curve has the horizontal slope T_S and T_K. The second section is best described by the so-called Kloss' equation [9]:

$$T(s) = \frac{2 \cdot s \cdot s_k \cdot T_K}{s^2 + s_k^2}, \quad (2)$$

where $s = 1 - n/n_{sk}$ is the slip at any point of the interval, $s_k = 1 - n_k/n_{sk}$ is the slip and n_k is the number of revolutions, both at the point of pull-out torque, while n_{sk} is the number of revolutions at synchronous speed. The modelled torque-speed curve of the squirrel cage motor KBF – 90 LA 2, according to Eqs. (1) and (2), is given in Fig. 5.

Starting an AC motor and its speed regulation are today successfully done by changing the frequency of the AC signal, f (e.g. using six-step inverter, pulse-width modulation, etc.). When a variable frequency drive starts a motor, it initially applies a low frequency and voltage to the motor. This avoids the high inrush current that occurs when a motor is started by simply applying the utility voltage by turning on a switch. This also allows a motor to develop 150 % of its rated torque while drawing only 50 % of its rated current. For the sake of comparison, when a motor is simply switched on at full voltage, it initially draws at least 300 % of its rated current while producing less than 50 % of its rated torque.

In order to obtain the torque-speed curve with frequency regulation one may use the relations yielding that the motor torque is proportional to the square of the flux developed in the motor ($T \sim \Phi^2$) and that the developed flux is proportional to the voltage, U, divided by the frequency, f, ($\Phi \sim U/f$) [10]. Those two relations result in a relation that describes the electric motor torque as a function of voltage and frequency:

$$T_K(U, f) = \left(\frac{U}{U_n}\right)^2 \cdot \left(\frac{f_n}{f}\right)^2 \cdot T_{KN}, \quad (3a)$$

where T_K is the pull-out torque at any voltage U and frequency f; U_n and f_n are the nominal values of voltage (U_n = 380 V) and frequency (f_n = 50 Hz) and T_{KN} is the pull-out torque at U_n and f_n.

The starting frequency is typically 2 Hz, or less. The frequency and voltage are further simultaneously increased at a controlled rate or ramped up to accelerate the load. This is done up to the frequency of 50 Hz and so as to keep the flux constant and maximal. In this manner, the value of the term $(U/U_n)^2 \cdot (f_n/f)^2$ in Eq. (3a) is kept equal to 1 and, hence, the motor delivers rated torque. Upon reaching the nominal values of voltage and frequency, U_n and f_n, further torque development is described by Kloss' equation (Eq. (2)) until the stationary work regime is reached, i.e. the work point WP, which is defined by the intersection of motor torque T_M and load torque T_W. In Fig. 6 curve (1), which consists of a straight line in the first section and the Kloss' curve in the second section, represents the corresponding torque-speed curve.

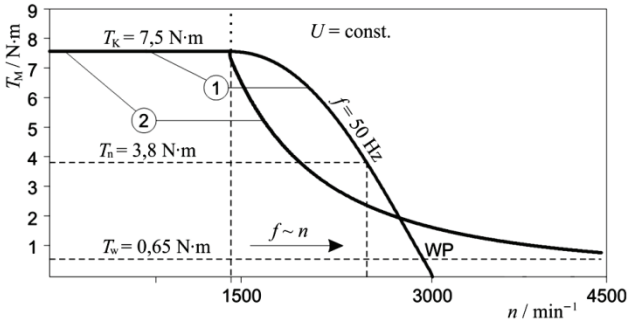

Figure 6 Modelled torque-speed curves of squirrel cage motor KBF – 90 LA 2

Variable frequency drive at the above synchronous speed is also possible, but is limited to the condition that not more power than nameplate rating of the motor is required. Hence, when the nominal voltage, U_n, is reached, with further increase of frequency above the nominal value, f_n, the flux decreases with f^{-1} and the torque with f^{-2}. According to Eq. (3a), above the synchronous speed, i.e. for f = 50 ÷ 100 Hz the electric motor torque follows the law:

$$T_K = \left(\frac{f_n}{f}\right)^2 \cdot T_{KN} = \left(\frac{n_k}{n}\right)^2 \cdot T_{KN}. \quad (3b)$$

Curve 2 in Fig. 6 depicts this torque development.

As for the excavator's drive mechanism, the electric motor has the nominal power of P_M = 250 kW, nominal speed of rotation n_1 = 985 1/min and characteristic torque values: T_A = 5,31 kN·m, T_S = 4,35 kN·m, T_K = 5,55 kN·m and T_n = 2,41 kN·m.

2.2.2 Modelling braking torque

Having considered modelling the electric motor torque, it would be worthwhile at this point to focus attention to modelling the torque exhibited by the brake. In the considered cases, the brake is placed on the side of equivalent model's driving mass and, therefore, its action has direct impact on the driving mass. For the type of brakes considered in the paper, the braking torque is usually described in a simplified manner by one of the following 3 functions in time (Fig. 7): constant (a), slope-combined (b) and exponential (c), and the corresponding relations are, respectively:

$$T_B = T_{B0} = \text{const.} \quad \text{for} \quad t \geq t_0, \quad (4)$$

$$T_B = \begin{cases} T_{B0} \cdot \dfrac{t - t_0}{t_A} & \text{for } t_0 \leq t \leq t_0 + t_A \\ T_{B0} & \text{for } t \geq t_0 + t_A \end{cases}, \quad (5)$$

$$T_{\mathrm{B}} = T_{\mathrm{B0}} \cdot \left(1 - \mathrm{e}^{-\frac{t-t_0}{t_{\mathrm{A}}}} \right) \quad \text{for} \quad t \geq t_0, \tag{6}$$

where T_{B0} is the maximum value of braking torque, t_A is time constant of braking torque development which can be regulated within the interval 0,06 ÷ 0,5 s and t_0 is time needed for the brake to start acting.

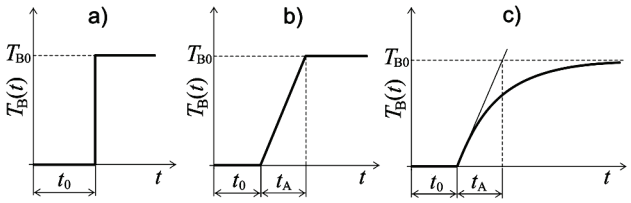

Figure 7 Brake torque development: a) constant, b) slope-combined and c) exponential

2.2.3 Modelling torques due to external forces

The external loads that act upon the executive parts of mechanisms are reflected in load torques acting on the driven mass of the equivalent torsional model given in Fig. 4, $T_2 = T_w$. They primarily depend on the task done by the drive mechanism.

In the first example that handles the movement mechanism of a crane (Fig. 1), the load torque depends on the force that resists the movement F_w:

$$T_{\mathrm{w}} = -F_{\mathrm{w}} \cdot \frac{D}{2}. \tag{7}$$

The force F_w consists of several components and it also depends on the crane environment, i.e. whether the crane operates indoor or outdoor. In the considered example the crane operates indoor and, hence, the force F_w is only due to friction and inclination of the wheels' axes with respect to the direction perpendicular to the rails [11]:

$$F_{\mathrm{w}} = \sum m_i \cdot g \cdot (w + \kappa), \tag{8}$$

where Σm_i denotes the overall translational mass (the crane and load together), g = 9,81 m/s^2, w is the specific resistance due to friction and κ is the empirical value of resistance due to inclination. In practical calculations, this torque is assumed to have a constant value and, hence, the same is done here, whereby the calculation yields T_w = – 22,4 N·m.

Considering the bucket wheel excavator, the load torque depends on digging resistance (its tangential component $F_T(\psi)$) and the bucket wheel diameter D_{RT}:

$$T_{\mathrm{w}} = -F_{\mathrm{T}}(\psi) \cdot \frac{D_{\mathrm{RT}}}{2}. \tag{9}$$

The process of digging by means of excavator is continuous, since in each time moment at least one bucket edge cuts the soil and the bucket gets loaded. The digging is realized by simultaneous rotation of the bucket wheel about its axis and rotation of the excavator's boom and the rotor in the horizontal plane. The overall force can be decomposed into three mutually perpendicular components: the component tangential to the trajectory of the cutting edge in the rotor's plane, $\vec{F}_{\mathrm{T}}$, the normal component $\vec{F}_{\mathrm{N}}$, which is perpendicular to both, the trajectory and $\vec{F}_{\mathrm{T}}$ in the rotor's plane, and, finally, the side component $\vec{F}_{\mathrm{B}}$, which is perpendicular to the rotor's plane, i.e. perpendicular to the components $\vec{F}_{\mathrm{T}}$ and $\vec{F}_{\mathrm{N}}$. Since the tangential component determines the load torque in this case, the attention will be focused on it. Actually, it will be shown how the cutting resistance, $F_C(\psi)$, as a main component of the digging resistance, is calculated.

The cutting resistance can be determined by multiplying specific linear cutting resistance k_l, which is characteristic of the soil, with the mean sum of the length of blade cutting edges l_{sr} which are in contact with the soil. However, since the specific cutting resistance k_l is a random value that depends on soil specifications, the cutting resistance cannot be represented as a single mathematical function. Hence, the following relation yields very good results for the cutting resistance [13]:

$$F_{\mathrm{C}}(\psi) = k_{\mathrm{l}} \cdot l_{\mathrm{sr}} \cdot f_{\mathrm{o}}(\psi), \tag{10}$$

where:

$$f_{\mathrm{o}}(\psi) = \begin{cases} \sin\psi \\ \dfrac{(\alpha - \psi)}{\left(\alpha - \dfrac{\pi}{2}\right)} \\ 0 \end{cases} \quad \text{for} \quad \begin{cases} 0 \leq \psi \leq \dfrac{\pi}{2} \\ \dfrac{\pi}{2} \leq \psi \leq \alpha. \\ \psi > \alpha \end{cases} \tag{11}$$

This relation was used to create the algorithm, which can be described in the following way:

1. defining the length of cutting edges (not discussed here),
2. defining the angular coordinate of rotor's revolution by using angular velocity ($\psi = \omega \cdot t$),
3. reducing angular coordinate to interval 0° ÷ 360°,
4. defining specific cutting resistance (k_l) as a value with random character,
5. determination of cutting resistance for every respective bucket,
6. summing resistances on all buckets which are simultaneously engaged in work on the massif.

Researches in this field [13] have shown that the specific cutting resistance k_l can be mathematically described by using the nominal law of distribution. Tab. 1 gives a review of mean values and standard deviation of value k_l obtained experimentally by performing measurements on a bucket wheel excavator operating on surface mining [14].

The specific cutting resistance is modelled by means of *Matlab*'s *randtool*. This tool automatically generates a set of random numbers according to predefined

distribution and sample size. With the values of specific cutting resistance and estimated active length of bucket's cutting edge, the block-scheme of the *Simulink* model generates cutting resistance for one bucket. The final step is summation of cutting resistances for single buckets so as to obtain the total cutting resistance. The influence of the mass of soil in the buckets is neglected in the scope of this research, as this influence is rather small compared to the above discussed cutting resistance. Fig. 8a depicts the modelled digging resistance F_T for one bucket based on data given in Tab. 1, while Fig. 8b shows the total digging resistance (F_{sum}) that acts upon the bucket-wheel.

Table 1 Specific digging resistance (experiment)

Digging environment	Mean value k_1 / N/cm	Standard deviation
Fault zone	436	104
Transitional zone	610	107
Gray clay	692	158

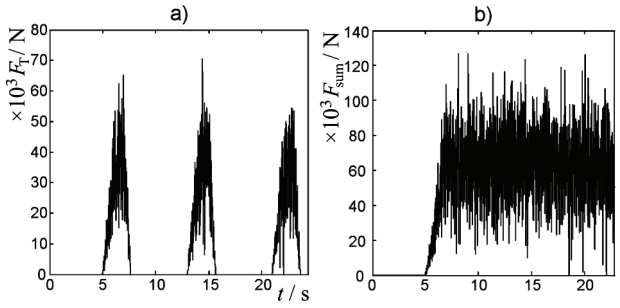

Figure 8 Modelled cutting resistance: a) one excavator's bucket and b) total resistance

2.3 Analytical model

Having defined the characteristics (J_1, J_2, b_1, c_1, φ_z) and components of external disturbances, T_1 and T_2, of the equivalent model with two revolving masses (Fig. 3), in the very next step an adequate mathematical model is derived. The masses of the model perform forced damped oscillatory motion in the transient work regimes (acceleration and braking) under the influence of external disturbances, i.e. the electric motor torque T_M, brake torque T_B and load torque T_W. Hence, the analytical description of the masses' motion is given by ordinary second-order non-homogeneous differential equations. They are derived for each phase of motion (given in Fig. 4) by applying d'Alembert's principle.

In the most general case, the period of acceleration under the influence of electric motor torque $T_1 = T_M$ and load torque $T_2 = -T_w$ consists of three phases: closing gap φ_z (Fig. 4a), elastic bond deformation (Fig. 4b) and asynchronous motion of both masses (Fig. 4c) till the end of the acceleration phase. Differential equations for all three above mentioned periods are, respectively:

$$J_1 \cdot \ddot{\varphi}_1 = T_M, \tag{12}$$

$$J_1 \cdot \ddot{\varphi}_1 + b_1 \cdot \dot{\varphi}_1 + c_1 \cdot \varphi_1 = T_M, \tag{13}$$

$$\begin{aligned} &J_1 \cdot \ddot{\varphi}_1 + b_1 \cdot (\dot{\varphi}_1 - \dot{\varphi}_2) + c_1 \cdot (\varphi_1 - \varphi_2) = T_M, \\ &J_2 \cdot \ddot{\varphi}_2 - b_1 \cdot (\dot{\varphi}_1 - \dot{\varphi}_2) - c_1 \cdot (\varphi_1 - \varphi_2) = -T_W. \end{aligned} \tag{14}$$

The first two phases can be neglected if the elastic bond of the model is preloaded. Upon the acceleration, both masses perform synchronous motion till the end of the stationary motion period.

In the next, braking period, the motor drive is switched off and the brake starts to act, thus causing the torque $T_1 = -T_B$. The braking process is similar to the asynchronous motion of the masses in the acceleration period (Fig. 4c) and it is described by a system of differential equations, similarly to Eqs. (14):

$$\begin{aligned} &J_1 \cdot \ddot{\varphi}_1 + b_1 \cdot (\dot{\varphi}_1 - \dot{\varphi}_2) + c_1 \cdot (\varphi_1 - \varphi_2) = -T_B \\ &J_2 \cdot \ddot{\varphi}_2 - b_1 \cdot (\dot{\varphi}_1 - \dot{\varphi}_2) - c_1 \cdot (\varphi_1 - \varphi_2) = -T_W. \end{aligned} \tag{15}$$

After the driving mass is stopped, within the models with $J_1 < J_2$ the driven mass oscillates around the balance position until it finally rests (Fig. 4d), which is described by the following differential equation:

$$J_2 \cdot \ddot{\varphi}_2 + c_1 \cdot \varphi_2 = -|T_W| \cdot \text{sign}\ \dot{\varphi}_2, \tag{16}$$

where sign $\dot{\varphi}_2$ has the value (+1) for $\dot{\varphi}_2 > 0$ and (–1) for $\dot{\varphi}_2 < 0$.

2.4 Laws of motion and loading functions

In the fourth phase of modelling, the differential equations of motion (Eqs. (12-16)) are solved in order to obtain the laws of motion and the load function of elastic bond. The solution for the initial conditions $\varphi_1(t_0) = \varphi_{10}$, $\dot{\varphi}_1(t_0) = \dot{\varphi}_{10}$, $\varphi_2(t_0) = \varphi_{20}$ and $\dot{\varphi}_2(t_0) = \dot{\varphi}_{20}$ at $t = t_0$ defines the laws of motion of each mass separately, $\varphi_1(t)$, $\dot{\varphi}_1(t)$, $\ddot{\varphi}_1(t)$ and $\varphi_2(t)$, $\dot{\varphi}_2(t)$, $\ddot{\varphi}_2(t)$. It should be noticed that the end-values of each period of motion are the initial values of the next period.

The elastic bond of the equivalent model, i.e. the referent shaft, is exposed to the following torque function:

$$T_{sh}(t) = c_1 \cdot [\varphi_1(t) - \varphi_2(t)] = c_1 \cdot \Delta\varphi(t), \tag{17}$$

where $\Delta\varphi(t) = \varphi_1(t) - \varphi_2(t)$ is the deformation of the elastic bond.

This concludes the procedure of modelling drive mechanisms of electric motor driven machines, which provides the basis for the simulation of their work under various exploitation conditions.

3 Drive mechanisms' work simulation

The work of drive mechanisms is simulated using the equivalent dynamic model (Fig. 4) and the corresponding analytical model given as a set of differential equations (Eqs. (12 ÷ 16)) that describe single movement periods. Upon linking the single movement periods one gets the simulation of the whole movement of drive mechanism, i.e. the laws of motion and elastic bond load function. This task is successfully solved by means of appropriate software packages. In what follows, simulations of

dynamic behaviour of the above considered two drive mechanisms are presented.

First, the drive mechanism of the laboratory apparatus (Fig. 1) is considered. The functions of mechanism velocity $v(t)$ and torque $T_{sh}(t)$ of the reducer output shaft, i.e. the wheel shaft, are sought for one movement consisting of acceleration period, stationary motion and braking. The characteristics of the equivalent model (Fig. 4), reduced to the wheel shaft, are: $J_1 = 27{,}35$ kg·m^2, $J_2 = 62{,}50$ kg·m^2, $c_1 = 24\,206$ N·m and $b_1 = 14{,}00$ N·m·s. The torque-speed curve of the squirrel cage motor (Fig. 5) is modeled by means of Eqs. (1) and (2). Within this analysis, the braking torque is considered to be constant (Fig. 7a) with the value $T_B = T_{ko} = -9{,}6$ N·m. Since the simulation is performed for the output shaft of the mechanism, the electric motor torque and the braking torque are reduced onto that shaft, in the following way:

$$T_{out} = T_{inp} \cdot i_R \cdot \eta$$
$$\dot{\varphi}_{out} = \frac{\dot{\varphi}_{inp}}{i_R} = \frac{\pi \cdot n}{30 \cdot i_R}. \qquad (18)$$

where T_{inp}, T_{out}, $\dot{\varphi}_{inp}$ and $\dot{\varphi}_{out}$ are the torques and the angular velocities before and after the reduction, respectively, $i_R = 35{,}5$ is the gear ratio and $\eta = 0{,}95$ is the reducer efficiency factor.

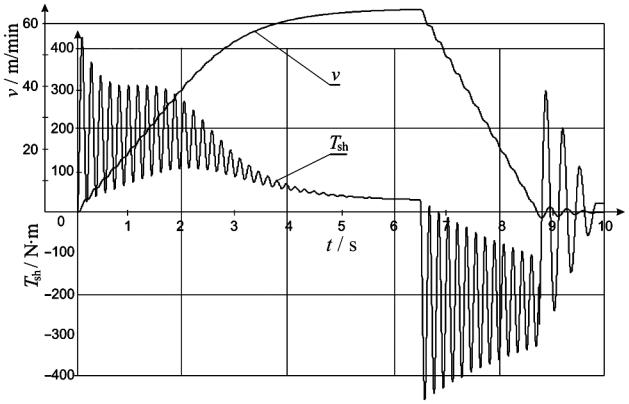

Figure 9 Simulation results for laboratory apparatus: mechanism velocity $v(t)$ and outlet shaft's torque $T_{sh}(t)$

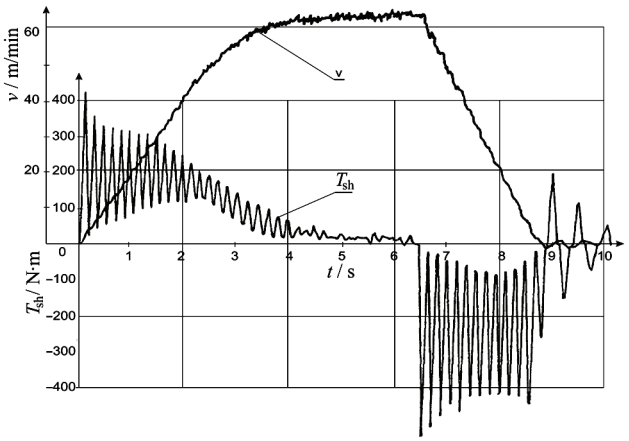

Figure 10 Experimental results for laboratory apparatus: mechanism velocity $v(t)$ and outlet shaft's torque $T_{sh}(t)$

Figs. 9 and 10 give the simulation and experimental results for the shaft torque, $T_{sh}(t)$, and for the velocity of the mechanism, $v(t)$, respectively. In the acceleration period the electric motor is directly started (i.e. no speed control). During the whole movement, the load torque, the value of which is $T_W = -22{,}4$ N·m, acts upon the driven mass in the direction opposite to the velocity. Finally, during the braking period, the brake torque directly acts upon the driving mass. Experimental results are obtained by performing measures on the laboratory apparatus. In order to measure the torque acting upon the shaft, four strain gauges are mounted on the shaft in the directions at 45° to the axis of the shaft since those directions experience stretch and compression due to torsion. The strain gauges are interconnected into a 'Wheatstone bridge' configuration to sense resistance changes produced in them and, hence, the output voltage is directly related to the shaft torque. The velocity of the mechanism is determined by means of a dc tachometer that was used to measure directly the number of revolutions per minute of the rail wheel.

On the curves in Figs. 9 and 10 one may distinguish the acceleration period (approximately up to $t = 5$ s), stationary motion ($t = 5 \div 6{,}5$ s) and braking period (after $t = 6{,}5$ s). The mean value of the shaft torque during the acceleration period resembles the starting characteristic of the electric motor. During the stationary motion, the shaft torque approaches slowly the value of the load torque, while the velocity flattens out becoming nearly constant. Two phases can be distinguished in the braking period. During the first phase ($t = 6{,}5 \div 8{,}8$ s) both masses decelerate asynchronously and the shaft torque is of opposite direction compared to the first two periods. Once the driving mass comes to rest, the driven mass performs further oscillations ($t > 8{,}8$ s). The shaft is exposed to torque of alternating direction.

One may notice a good agreement between experimental and simulation results. It should be emphasized that the gap in the mechanism is closed in the beginning of the experiment (preloaded mechanism). The most significant differences between the experimental and simulation results are seen in the second phase of braking period, i.e. for the time period after $t = 8{,}8$ s. The reason for this is the fact that the gap is not considered in the simulation and this phase is strongly affected by the gap since the mechanism goes through it in each single oscillation. The gap causes longer periods of oscillations than predicted by the simulation as well as stronger damping of the oscillations due to energy dissipation caused by impacts that occur every time the gap is closed. Furthermore, the simulation results in Figs. 9 and 10 are obtained by considering the movement resistance to be constant. However, the experimental results reveal that this is actually not the case. Therefore, the simulation is repeated with the movement resistance modelled as a random quantity with normal distribution, the mean value and standard deviation of which are 22,4 N·m and 10 N·m, respectively.

Fig. 11 shows the simulation results in this case for the period of up to 6,5 s. The period of stationary motion is mostly affected by the stochastic nature of resistant forces. This is best seen in the way in which the torque and velocity change in the time period t = 4 ÷ 6,5 s.

Fig. 12 depicts the torque that acts upon the shaft in the case when a variable frequency drive is used to start

the motor (curve 1 in Fig. 6). Only the acceleration period is shown (f = 2,5÷50 Hz), since it demonstrates the advantages of the variable frequency drive.

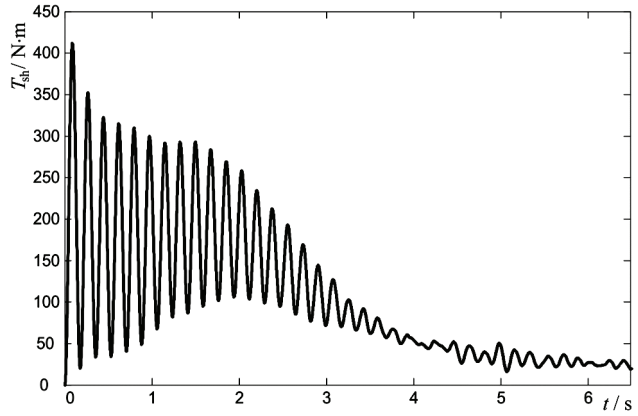

Figure 11 Simulation results for laboratory apparatus: outlet shaft's torque $T_{sh}(t)$ with movement resistance as random quantity

The attention is further focused on the example dealing with the bucket-wheel excavator (Fig. 2). The subject of interest is the load function, i.e. the torque, that acts upon the first (inlet) shaft, $T_{sh}(t)$. The considered period of work consists of two phases. In the first phase, the mechanism is started and accelerated, whereby the buckets are not in contact with the soil. Once the mechanism is up to speed, the buckets of the wheel start the digging process. The characteristics of the equivalent model are J_1 = 27 kg·m^2, J_2 = 8,2 kg·m^2, b_1 = 0 N·m·s and c_1 = 1608 N·m.

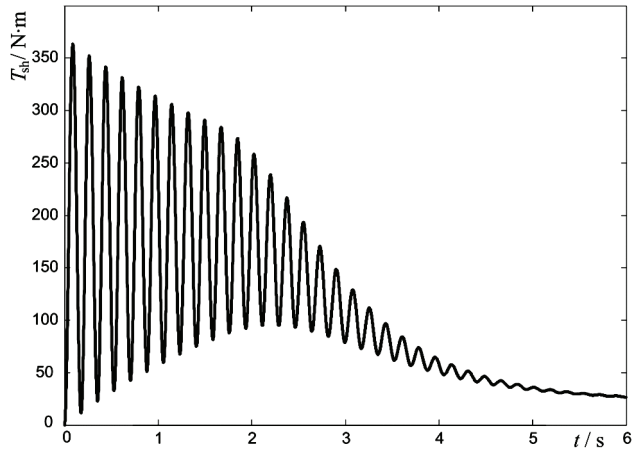

Figure 12 Simulation results for laboratory apparatus: outlet shaft's torque $T(t)$ with a variable frequency drive

Fig. 13 shows the studied shaft torque during the period of 30 s, the first 5 s of which belong to the acceleration phase and the rest involve the digging process. The obtained diagram is a result of simulation. An experiment would be rather expensive in this case. In the acceleration phase the inertia of the system plays the main role, whereas in the second phase the digging resistance becomes the primary force to overcome. The two phases are clearly distinguishable in the diagram. The electric motor torque acts during the whole period. From the diagram one may read the maximal torque of T_{max} = 2646 N·m, minimal torque of T_{min} = –1108 N·m and the mean value of T_{mean} = 1337 N·m. As can be seen, the shaft torque takes also negative values during the acceleration phase. This is a consequence of the fact that there are no resistant forces acting upon the driven mass (J_2). Hence, towards the end of the acceleration phase the value of the shaft torque oscillates around zero. In further analysis, the authors have applied the rainflow method in order to perform cycle counting and to obtain amplitudes T_{ai} and mean values T_{mi} of single cycles. The so-obtained spectrum of varying load has an important role in life-time estimation of shafts and other parts. For the sake of brevity, those results are not presented in this paper.

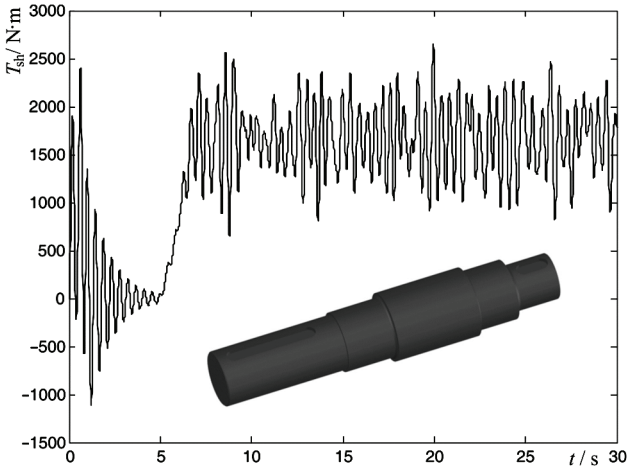

Figure 13 Simulation results for bucket-wheel excavator: torque upon the first shaft (T_{sh})

4 Conclusions

The paper revisits a simplified approach based on equivalent torsional models for modelling electric motor driven mechanisms. The models consist of a few (typically two or three) revolving masses connected with elastic bonds, the stiffness and damping properties of which reflect the properties of actual shafts of the mechanisms. The steps of deriving the model's parameters are discussed. A significant part of the paper addresses the problem of accurate description of electric motor torque and load torque due to resistant forces.

Dynamic behaviour of drive mechanisms of a crane and a bucket wheel excavator is investigated using the presented approach. Both experimental and simulation results are provided for the driving mechanism of the crane. A good agreement between them demonstrates that torques acting upon shafts and speed of rotation of single masses can be determined with satisfying accuracy, provided external disturbances are accurately described and the applied model well captures system characteristics once they are reduced with respect to the reference shaft. Furthermore, since the random character of resistant forces may play a significant role in dynamics of some machines, this aspect is also considered in the paper for both investigated mechanisms. It is obvious that the aspect is more significant in the case of bucket wheel excavator, thus requiring statistics in order to perform more detailed assessment of the obtained results.

The presented approach is suitable for resolving global dynamic behaviour of mechanisms, i.e. it does not provide detailed insight into mechanical behaviour of mechanism elements (e.g. induced strain and stress states,

etc.). But it requires only a few system parameters that approximately describe its elements' global properties (stiffness, inertia, damping, and gap) and it is rather inexpensive in terms of modelling and numerical effort. Therefore, it is well suited only for the preliminary design phase, during which the precise knowledge of geometry of mechanisms' elements still lacks. It is also most suitable for the input shafts of the mechanisms, as the mechanical behaviour of the output shafts can be noticeably affected by the mechanical behaviour of the carrying structure. The obtained results offer a solid base for assessment of conceptual design of mechanisms. The simplicity and efficiency of approach gain in importance when a set of influencing parameters are varied with the aim of conducting multi-variant design, in order to abandon designs that do not comply with predefined requirements and to point out those designs that are likely to give the optimal solution.

As it was recognized in the example that considers the crane, accounting for gap in mechanisms would improve the accuracy of results, especially in certain movement phases. Part of the future authors' work will be to develop a program for time integration of the governing differential equations that could also consider gap in mechanisms.

Acknowledgment

This paper is supported by the Ministry of Science of the Republic of Serbia, Project Nr. 35049. This support is gratefully acknowledged.

5 References

[1] Qin, W.; Dong, D. Study on Dynamics Analysis of Powertrains and Optimization of Coupling Stiffness. X. T. Yan, W. J. Ion and B. Eynard (Eds.) Global Design to Gain a Competitive Edge An Holistic and Collaborative Design Approach based on Computational Tools, Springer London, 2008.

[2] Avilés, R.; Hernández, A.; Amezua, E.; Altuzarra O. Kinematic analysis of linkages based in finite elements and the geometric stiffness matrix. Mechanism and Machine Theory, 43, (2008), pp. 964–983.

[3] Wilson, W. K. Practical solution of torsional vibration problems. Chapmann & Hall Ltd., London, 1963.

[4] Hafner, E. K.; Maass H. Theorie der Triebwerks-schwingungen der Verbrennungs-kraftmaschine. Springer - Verlag, Wien, New York, 1984.

[5] Dresig, H. Schwingungen mechanischer Antriebs-systeme – Modellbildung, Berechnung, Analyse, Synthese. Springer Verlag, Berlin Heidelberg, 2001.

[6] Marinković, Z.; Petrović, G. Processing the life time of bucket wheel excavator parts in strip mine technologies. // Scientific Journal Facta Universitatis, series Mechanical Engineering, 2, 1(2004), pp. 109–124.

[7] Vladić, J.; Đokić, R.; Kljajin, M.; Karakašić, M. Modelling and simulation of elevator dynamic behavior. // Tehnicki Vjesnik – Technical Gazette, 18, 3(2011), pp. 423–434.

[8] Marghitu, D. B. (Ed.) Mechanical Engineer's Handbook. Academic Press, 2007.

[9] Buscher, M. Radschlupfregelung zur maximalen Kraft-schlussausnutzung bei elektrischen Traktionsantrieben. PhD thesis, Technische Hochschule Darmstadt, Shaker Verlag, Aachen, 1995.

[10] Basics of AC Drives, Siemens STEP 2000 Course. Siemens Technical Education Program, from http://www.scribd.com /doc/7735240/Basics-AC-DriveSiemens, accessed on 2011-04-20.

[11] Scheffler, M.; Pajer, G.; Kurth, F. Grundlagen der Fördertechnik – Einführung, Bauteile und Maschinensätze, Grundlagen des Stahlbaus. VEB Verlag Technik, Berlin, 1968.

[12] Pajer, G.; Kurth, F.; Pfeifer, M.; Hojdar, J. Tagesbaugroß-geräte und Universalbagger. VEB Verlag Technik, Berlin, 1979.

[13] Arsić, M.; Ljamić, D.; Ćirković, B. Experimental Analysis of the Workload of the Excavator's Bucket Wheel Drive. // Proceedings of IRMES '95, (1995), pp. 346–351.

[14] Petrović, G.; Marinković, Z.; Marinković, D. Modeling and Simulation of the Operation of Excavator's Bucket Wheel Driving Mechanism. // Proceedings of 13th International Conference on Material Handling, Constructions and Logistics, 2006.

Authors' addresses

Prof. dr Zoran Marinković
University of Niš, Faculty of Mechanical Engineering
A. Medvedeva 14, 18000 Niš, Serbia
E-mail: zoranm@masfak.ni.ac.rs

Dr Dragan Marinković, docent
Technical University Berlin, Institute of Mechanics
Straße des 17. Juni 135, 10623 Berlin, Germany
E-mail: Dragan.Marinkovic@TU-Berlin.de

Mr Goran Petrović
University of Niš, Faculty of Mechanical Engineering
A. Medvedeva 14, 18000 Niš, Serbia
E-mail: pgoran@masfak.ni.ac.rs

Predrag Milić
University of Niš, Faculty of Mechanical Engineering
A. Medvedeva 14, 18000 Niš, Serbia
E-mail: predragmilic@yahoo.com